European Journal of Pharmaceutics and Biopharmaceutics 145 (2019) 113–120

Contents lists available at ScienceDirect

European Journal of Pharmaceutics and Biopharmaceutics

journal homepage: www.elsevier.com/locate/ejpb

Research paper

Solubility of pharmaceutical ingredients in triglycerides

Joscha Brinkmann, Fabian Huxoll, Christian Luebbert, Gabriele Sadowski*

Laboratory of Thermodynamics, TU Dortmund University, Emil-Figge-Str. 70, D-44227 Dortmund, Germany

ARTICLE INFO

Keywords:
Lipid-based drug delivery systems
Triglycerides
Solubility
Phase diagram
Thermodynamic modeling
PC-SAFT

ABSTRACT

Lipid-based drug delivery systems (LBDDS) are highly relevant as pharmaceutical formulations significantly enhancing the bioavailability of active pharmaceutical ingredients (APIs). These formulations often are complex mixtures of APIs, various lipids, and other excipients (e.g. surfactants). In their simplest form, LBDDS contain one API being dissolved in a pure lipid, which often is a triglyceride (TG). In this work, solubilities of the APIs indomethacin, ibuprofen, and fenofibrate in pure TGs of different chain lengths (C chain 8–18) and degree of saturation were investigated. Solubilities of APIs in TGs were measured via differential scanning calorimetry, hot-stage microscopy, high-performance liquid chromatography, and Raman spectroscopy. The influence of fatty-acid chain length and degree of saturation on the API solubility in the TGs was investigated. APIs showed a higher solubility in saturated (w_{IBU} = 10.5 wt% at 25 °C in tricaprylin) TGs compared to unsaturated ones (w_{IBU} = 4.0 wt% at 25 °C in triolein). The fatty-acid chain length of TGs only slightly affects the solubility of ibuprofen and fenofibrate, but strongly influences the eutectic temperature of the API/TG mixtures.

API solubilities in TGs and TG mixtures (mixtures of tricaprylin and tricaprin) were successfully modeled using the Perturbed-Chain Statistical Associating Fluid Theory (PC-SAFT) accounting for the intermolecular API/TG interactions providing a deep understanding of the energetic and structural impact of the TGs on API solubility.

1. Introduction

Many newly-developed active pharmaceutical ingredients (APIs) have a low bioavailability which often is caused by their extremely low water solubility [1]. One approach to increase the bioavailability is to apply innovative formulations like lipid-based drug delivery systems (LBDDS), in which APIs are dissolved in lipids. Lipids used for that type of formulations usually are triglycerides (TGs), diglycerides, monoglycerides, or mixtures thereof [2–4]. Chemically, TGs comprise one glycerol backbone and up to three fatty-acid ester groups, which can differ in carbon chain lengths and/or degree of unsaturation [4]. Typically-used lipids for pharmaceutical formulations are natural edible oils (e.g. soybean oil), consisting of a complex mixture of hundreds of different TGs. Nowadays, new LBDDS are developed via trial-and-error methods. Due to the large variety of possible APIs, lipids and further excipients, these methods are not very straight forward and result in very expensive and time-consuming procedures [3,5–7].

Moreover, the maximum API load in an LBDDS is limited by the solubility of the API in the TG. In recent studies the solubility of a broad range of APIs in commonly-used excipients for LBDDS has been investigated [5,8,9]. Experimental state-of-the-art methods for that purpose comprise HPLC [10,11], UV–Vis spectrometry [5] and differential scanning calorimetry (DSC) [12]. However, to the best of our knowledge, there has never been a work, focusing on the structural impacts of TGs on the API solubilites.

Moreover, so far only empirical approaches were used to correlate the solubility of APIs in LBDDS. These correlations do neither allow for extrapolations to other TGs or TG mixtures nor for structural insights in what TG properties are decisive to enhance API solubilities [13]. In order to improve the development of new LBDDS and to better understand the impact of the TG structure on API solubility, the physically-sound Perturbed-Chain Statistical Associating Fluid Theory (PC-SAFT) was applied in this work for correlating and even predicting API solubilities. PC-SAFT has already been successfully applied in the past for calculating thermodynamic properties of other pharmaceutical formulations [14,15] and will in this work for the first time be applied to calculate API solubilities in pure TGs and TG mixtures.

* Corresponding author.
E-mail address: gabriele.sadowski@tu-dortmund.de (G. Sadowski).

https://doi.org/10.1016/j.ejpb.2019.10.012
Received 7 June 2019; Received in revised form 26 August 2019; Accepted 22 October 2019
Available online 02 November 2019
0939-6411/ © 2019 Elsevier B.V. All rights reserved.

Nomenclature

a	Helmholtz energy (J mol^{-1})
h	molar enthalpy (J mol^{-1})
c_p	heat capacity (J mol^{-1} K^{-1})
k_B	Boltzman constant (J K^{-1})
k_{ij}	binary interaction parameter (–)
M	molar mass (g mol^{-1})
m_i^{seg}	segment number (–)
N_i^{assoc}	number of association sites (–)
R	ideal gas constant (J mol^{-1} K^{-1})
T	temperature (°C)
$u_i k_B^{-1}$	dispersion energy parameter (K^{-1})
w_i	mass fraction (wt%)
x_i	mole fraction (mol%)

Greek characters

γ	activity coefficient (–)
$\varepsilon_i^{AiBi} k_B^{-1}$	association energy (K^{-1})
κ^{AiBi}	association volume (–)
σ_i	segment diameter (Å)

Subscripts

eut	eutectic
i	component
int	intersection
0	pure component

Superscripts

assoc	associating
disp	dispersion
hc	hard chain
L	liquid
res	residual
S	solid
seg	segment

2. Materials and methods

2.1. Materials

Tricaprylin (a TG with three fatty-acid chains, each having a chain length of eight and no double bonds, thus abbreviated $TG8_08_08_0$ as in [16]) and tristearin ($TG18_018_018_0$) were purchased from Sigma Aldrich (Steinheim, Germany) with purities greater than 99%. Tricaprin ($TG10_010_010_0$) and trilaurin ($TG12_012_012_0$) were obtained from abcr GmbH (Karlsruhe, Germany) with a minimal purity of 98%. Triolein ($TG18_118_118_1$) and Trilinolein ($TG18_218_218_2$) were purchased with purities greater than 99% from Nu-Chek-Prep, Inc. (Elysian, Minnesota). The APIs fenofibrate (FFB), indomethacin (IND), and ibuprofen (IBU) were obtained from Tokyo Chemical Industry (Tokyo, Japan) with purities better than 98%.

2.2. Solubility measurements

Solubility temperatures in API/TG mixtures with high API loadings were determined via DSC experiments. For that purpose, approximately 100 mg of the API/TG mixtures were weighted in the desired ratio into a Mini-Pulverisette 23 from Fritsch (Idar-Oberstein, Germany) and milled for 20 min at a frequency of 40 Hz. The milled API/TG mixture were filled into hermetically-sealed aluminum pans and analyzed in a Q2000 DSC with RCS90 cooling device from TA Instruments (Eschborn, Germany). The DSC cell was purged with 50 mL min^{-1} nitrogen. A heating-cooling-heating procedure was conducted in a temperature range between at least 10 °C above the pure APIs' melting temperature and minimal 10 °C below the melting temperature of the TG. The solubility temperature of each API/TG system was determined via DSC measurements at different heating ramps (1 K min^{-1}, 2 K min^{-1} and 5 K min^{-1}). The solubility temperatures were then determined via evaluating the off-set melting-peak temperatures and extrapolated to a theoretical heating ramp of 0 K min^{-1} with an estimated uncertainty of ± 1 K [17].

Phase transitions (dissolution/melting and crystallization) of the considered API/TG mixture during heating and cooling were also observed visually via hot-stage microscopy (HSM). A Linkam THMS600 hot stage (Tadworth, United Kingdom) in combination with a Leica DM4000M microscope (Wetzlar, Germany) was used for that purpose.

For solubility measurements at 25 °C, a supersaturated sample of an API in a TG was shaken in an Eppendorf ThermoMixer C (Hamburg, Germany) at constant temperature for at least three days. Subsequently, the dispersed crystals were sedimented for at least three days, the supernatant was filtered with a 0.45 µm CHROMAFIL® Xtra PTFE-45/13 by Macherey-Nagel (Düren, Germany) and was then analyzed with HPLC or Raman spectroscopy.

For determining the API solubilities in $TG8_08_08_0$ with Raman-spectroscopy measurements were performed using a HORIBA LabRAM Raman spectroscope (Bensheim, Aachen) in combination with an Olympus IX 71 inverted microscope (Tokyo, Japan). Raman spectra of the saturated solutions were quantified by Indirect Hard Modeling as described in a recent work [18] using the PEAXACT 4 software (S–PACT, Aachen, Germany). Solubilities measured with Raman spectroscopy were determined with an uncertainty of ± 0.6 wt% according the calibration displayed in Fig. S1 in the Supporting Information. Each solubility experiment via Raman spectroscopy was conducted once.

For solubility measurements using high-performance liquid chromatography (HPLC), the saturated and filtered API/TG mixtures were diluted with pure acetonitrile to avoid API precipitation and to obtain an optimal UV–vis signal of FFB. An Agilent 1200 HPLC (Santa Clara, USA) was combined with a ZORBAX Eclipse XDB-C18 reversed phase column by Agilent (Santa Clara, USA). The mobile phase contained acetonitrile and an aqueous solution of phosphoric acid (70/30 v/v) with pH = 2.5. The flow rate was 1 mL min^{-1} with a column temperature of 35 °C. The API content was measured using a UV–vis detector at 286 nm for FFB and 225 nm for IBU, wavelength. For solubility measurements via HPLC, two independent experiments were conducted and the results were averaged. The uncertainty of the whole experimental procedure was found to be ± 0.3 wt%.

Details of all calibration procedures are given in the Supporting Information (Figs. S1 and S2). The data-point values shown later in this work are given in Tables S1–S4 of the Supporting Information.

Powder X-Ray diffraction (PXRD) was used to identify the different polymorphic forms of IND occurring during the DSC measurements. For that purpose, DSC measurements were interrupted at considered temperatures and the IND/$TG10_010_010_0$ samples from the DSC pans were immediately transferred to a silicon wafer and characterized with a Miniflex 600 PXRD device by Rigaku (Tokyo, Japan) in the 2Θ range $2° < 2\Theta < 30°$.

2.3. Solubility modeling

The API solubility in a TG can be discussed based on API/TG phase diagrams, as schematically depicted in Fig. 1.

API/TG mixture phase diagrams are divided into four characteristic

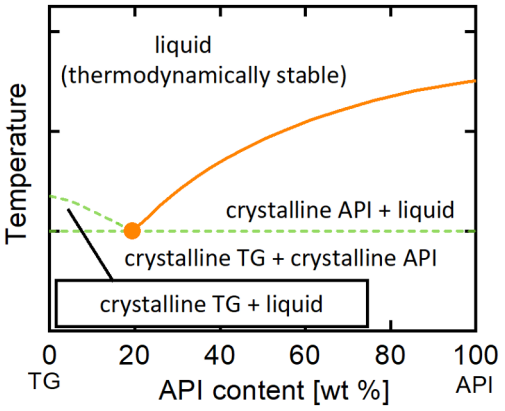

Fig. 1. Schematic phase diagram of a binary API/TG mixture. The relevant API solubility in the TG follows the solid line, the dashed lines are solubility lines not relevant in this work (solubility of the TG in API and the eutectic line). The circle is the eutectic point.

regions by solubility lines (in Fig. 1). All API/TG mixtures stored in the temperature/composition range above the solubility lines are homogeneous liquids. Below the solubility lines, either TG, API, or both API and TG crystallize. API/TG mixtures are preferably liquid at room temperature when applied as LBDDS and therefore should be stored at temperatures which lead to the thermodynamically stable, liquid area. The solubility line of the API in TG (right hand-side of Fig. 1) intersects with the solubility line of the TG in API (left hand-side of Fig. 1) in the eutectic point. Below the eutectic temperature, crystalline API as well as crystalline TG exist at the same time. The solubility lines of API in TG and vice versa are calculated using Eq. (1) [19].

$$x_i = \frac{1}{\gamma_i}\cdot\exp\left[-\frac{\Delta h_{0i}^{SL}}{R\cdot T}\cdot\left(1-\frac{T}{T_{0i}^{SL}}\right)-\frac{\Delta c_{p,0i}^{SL}}{R}\left[\ln\left(\frac{T_{0i}^{SL}}{T}\right)-\frac{T_{0i}^{SL}}{T}+1\right]\right] \quad (1)$$

The solubility x_i at a certain temperature T depends on the melting properties of the pure component i (either API or TG), namely its melting temperature T_{0i}^{SL}, melting enthalpy Δh_{0i}^{SL}, and on the difference of the heat capacities of the component as solid and liquid $\Delta c_{p,0i}^{SL}$. R is the ideal gas constant (8.1345 J mol^{-1} K^{-1}). Activity coefficients γ_i account for the non-ideal interactions in mixtures and were calculated in this work via PC-SAFT [20]. Both, the solubility of a TG in an API and the solubility of an API in a TG were calculated using Eq. (1), leading to the left and the right branch of the phase diagram in Fig. 1, respectively.

Table 1 summarizes the melting properties of the components investigated in this work. Melting properties of $TG12_012_012_0$, $TG16_016_016_0$ and $TG18_018_018_0$ were taken from literature [21], $\Delta c_{p,0i}^{SL}$ was set to zero for all TGs considered in this work.

PC-SAFT [20,23,24] calculates the residual Helmholtz energy a^{res} and was further used to calculate the activity coefficients in Eq. (1). Three different contributions to a^{res} were taken into account as shown in Eq. (2).

$$a^{res} = a^{hc} + a^{disp} + a^{assoc} \quad (2)$$

The three terms consider the different molecular interactions between molecules. Herein, a^{hc} stands for the hard-chain reference contribution accounting for repulsive interactions, a^{disp} accounts for attractive van-der-Waals interactions and a^{assoc} accounts for the associating interactions via formation of hydrogen bonds [20,23].

PC-SAFT considers a molecule as a chain with a certain number of identical spherical segments. For describing a molecule via PC-SAFT, three pure-component parameters have to be adjusted, namely the segment number m_i^{seg}, the segment diameter σ_i, and the dispersion-energy between two segments $u_i\ k_B^{-1}$ (whereas k_B is the Boltzmann constant). Associating molecules additionally require two pure-component parameters: the association energy $\varepsilon^{AiBi}\ k_B^{-1}$ and the association volume κ^{AiBi}. All PC-SAFT pure-component parameters for the considered TGs were taken from a recent work [16]. For reasonably describing interactions with associating molecules (APIs), TGs were considered as induced-associating with three proton donators and three proton acceptors per molecule [24,25].

PC-SAFT parameters for FFB were fitted to solubility data in organic solvents from literature [26] (solubility data and one example for fitting this data are shown in Figs. S3 and S4 of the Supporting Information, respectively). Due to its molecular structure, FFB is assumed to possess two association acceptor sites and no association donor site. FFB is considered as an induced-associating component [24]. For all TGs and FFB the association energy $\varepsilon_i^{AiBi}\ k_B^{-1}$ was set to zero and the association volume κ^{AiBi} was set to 0.02 [24]. Table 2 summarizes the pure-component parameters fitted in this work for FFB and the already known pure-component parameters of the other APIs which were taken from literature.

The dispersion energy u_{ij} among segments of two unlike molecules is obtained from the mixing rule given in Eq. (3).

$$u_{ij} = (1-k_{ij})\cdot\sqrt{u_i\cdot u_j} \quad (3)$$

k_{ij} is a binary interaction parameter correcting for deviations from the geometric mean and might linearly depend on temperature (Eq. (4)).

$$k_{ij}(T) = k_{ij,slope}\cdot T[K] + k_{ij,int} \quad (4)$$

The k_{ij}-value was fitted to experimental data (e.g. experimental solubility data from DSC measurements). Table 3 summarizes all the fitted binary interaction parameters k_{ij} used in this work.

3. Results

3.1. Solubility data obtained from different experimental methods

The experimental methods DSC, Raman spectroscopy, HPLC, and HSM measurements were combined to determine the solubility of FFB in $TG8_08_08_0$. The experimental values for FFB in $TG8_08_08_0$ as well as the modeling results obtained from PC-SAFT are given in Fig. 2.

DSC measurements were conducted for the high-API-loaded formulations, leading to data points at high temperatures and API compositions. These measurements revealed that the solubility temperatures decrease from the pure FFB's melting temperature of 80.6 °C to a solubility temperature of 69.0 °C in a formulation containing 40 wt% (measurements at lower FFB contents could not clearly be evaluated). Another FFB/$TG8_08_08_0$ sample with 20 wt% FFB was ball milled and heated with HSM under the microscope. The dissolution of all FFB crystals was optically observed at a temperature of 52 °C. The solubility of FFB/$TG8_08_08_0$ at 25 °C was measured via Raman spectroscopy and was found to be 9.9 wt%. This value is slightly higher than the result obtained from the HPLC measurements (8.3 wt% at 25 °C and 9.2 wt%

Table 1
Melting properties of APIs and TGs investigated in this work.

Component	Abbreviation	T_{0i}^{SL} [°C]	Δh_{0i}^{SL} [kJ mol^{-1}]	$\Delta c_{p,0i}^{SL}$ [J mol^{-1} K^{-1}]	source
Ibuprofen	IBU	77.1	25.5	50.3	[14]
γ-Indomethacin	γ-IND	160.2	39.3	117.0	[17]
α-Indomethacin	α-IND	152.0	34.7	*117.0	[22]
Fenofibrate	FFB	80.8 X	33.5	124.3	[26]
Tricaprylin	$TG8_08_08_0$	12.6	73.9 (± 2.0)	–	X
Tricaprin	$TG10_010_010_0$	33.2	119.6 (± 4.2)	–	X
Trilaurin	$TG12_012_012_0$	46.3	193.3	–	[21]
Tripalmitin	$TG16_016_016_0$	65.7	222.2	–	[21]
Tristearin	$TG18_018_018_0$	72.5	228.0	–	[21]

[x]this work, *assumed being the same for the two polymorphs

Table 2
PC-SAFT pure-component parameters for the APIs FFB, IBU, IND, the even, saturated TGs from $TG8_08_08_0$ to $TG18_018_018_0$ and the unsaturated TGs $TG18_118_118_1$ and $TG18_218_218_2$.

Abbreviation	M [g mol^{-1}]	m_i^{seg} [–]	σ_i [Å]	$u_i\ k_B^{-1}$ [K]	$\varepsilon_i^{AiBi}\ k_B^{-1}$ [K]	κ^{AiBi} [–]	N_i^{assoc} [–]	Ref.
FFB	360.80	3.859	4.767	244.8	0	0.02	0/2	X
IBU	206.28	2.522	4.432	374.7	879.4	0.03	2/2	[27]
IND	357.79	14.283	3.535	262.8	886.4	0.02	3/3	[17]
$TG8_08_08_0$	470.69	9.482	4.24	281.6	0	0.02	3/3	[16]
$TG10_010_010_0$	554.86	11.283	4.26	277.9	0	0.02	3/3	[16]
$TG12_012_012_0$	639.02	13.282	4.24	272.9	0	0.02	3/3	[16]
$TG16_016_016_0$	807.32	16.952	4.25	269.4	0	0.02	3/3	[16]
$TG18_018_018_0$	891.48	18.406	4.27	266.4	0	0.02	3/3	[16]
$TG18_118_118_1$	885.43	23.383	3.89	239.0	0	0.02	3/3	[16]
$TG18_218_218_2$	879.41	22.607	3.86	228.6	0	0.02	3/3	[16]

[x]This work.

Table 3
Binary interaction parameters k_{ij} of all binary systems considered in this work.

API	IBU		FFB		IND	
TG	$k_{ij,slope}$ [K^{-1}]	$k_{ij,int}$ [–]	$k_{ij,slope}$ [K^{-1}]	$k_{ij,int}$ [–]	$k_{ij,slope}$ [K^{-1}]	$k_{ij,int}$ [–]
$TG8_08_08_0$	0.00056	−0.183	0.00030	−0.1073	–	0.024
$TG10_010_010_0$	–	−0.018	–	–		
$TG12_012_012_0$	–	−0.018				
$TG16_016_016_0$	–	−0.018				
$TG18_018_018_0$	–	−0.018	0.00030	−0.1073		
$TG18_118_118_1$	–	0.008	–	0.007		
$TG18_218_218_2$	–	0.008	–	0.015		

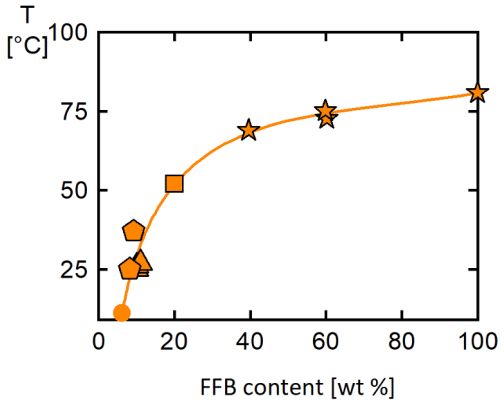

Fig. 2. Solubility FFB in $TG8_08_08_0$. Stars are values measured by DSC, triangles are solubilities determined via Raman spectroscopy, the pentagons were obtained by HPLC and the square was determined via HSM. The circle marks the calculated eutectic point. The solid line is the PC-SAFT calculation.

at 37 °C) but still shows the high accordance of the experimental methods.

All measurements perfectly agree to each other and cover the entire temperature range from 25 °C to 80 °C. Using the pure-component parameters from Table 2 and the binary interaction parameter from Table 3, PC-SAFT is able to quantitatively describe the solubility over the entire temperature/concentration range. The PC-SAFT-calculated eutectic point of FFB/$TG8_08_08_0$ is 11.6 °C at a composition of w_{FFB} = 6.8 wt%. Due to absence of a liquid phase solubility measurements below the eutectic point are not feasible.

At a temperature of 37 °C, the modeled FFB solubility is 13.2 wt%. This result again is in very good accordance to a literature solubility value of FFB in a commercial blend of TGs in which the solubility is about 18.0 wt% [10].

3.2. Solid state analysis of IND polymorphs in TGs

The DSC signals of IND/TG mixtures revealed different melting and recrystallization events, indicating the formation of different polymorphic forms of IND. HSM and PXRD measurements were conducted to understand which polymorph of IND occurred during heating. Fig. 3 shows PXRD diffractograms and HSM images of the binary system IND/$TG10_010_010_0$. A sample from DSC was analyzed at 22 °C during the first heating and at 86 °C during the second heating after recrystallization.

The comparison of the obtained diffractograms (Fig. 3c and d) with literature diffractograms of IND polymorphs [22,28,29] reveals that the initially present γ-IND did not change upon ball milling (Fig. 3a and c). According to the DSC and HSM measurements, the γ-IND in the IND/$TG10_010_010_0$ mixture with w_{IND} = 50 wt% melted at a temperature of 154.7 °C. The sample was subsequently quenched to 10 °C and reheated in a second heating ramp (see section *solubility measurements*). During the second heating ramp, recrystallization was observed in the heat flow signal. The HSM analysis (Fig. 3b) and PXRD analysis (Fig. 3d) proofed that IND recrystallized into the α-polymorphic form during the second heating of the sample. After recrystallization into the α-polymorphic form, the API/TG mixture melted at 148.2 °C.

The different polymorphic forms with different melting behavior were precisely identified and their different melting properties were explicitly taken into account in the modeling.

3.3. Influence of API type on the solubility in TGs

Solubilities of IND, FFB, and IBU in $TG10_010_010_0$ were determined via DSC measurements and are shown in Fig. 4a. The solubility of a crystalline API in a TG is influenced by both, its melting properties and the intermolecular interactions between API and TG (see Eq. (1)). The latter are described by the API activity coefficients which were calculated using PC-SAFT. The solubility of α-IND was predicted using the same pure-component parameters and binary interaction parameters as for the γ-form only using the melting temperature and enthalpy of α-IND as it has been done in recent works [30].

It can be seen in Fig. 4a that for each API and polymorph, there is a different starting point of the solubility line on the right side of the phase diagram, corresponding to the different melting points of the pure APIs/polymorphs. With decreasing API content, the melting temperatures of the mixtures decrease with a different slope for each API. Binary interaction parameters (Table 3) were fitted to these experimental data and solubilities of APIs at lower temperatures were then calculated by extrapolating with PC-SAFT. At 37 °C, solubilities of 6.8 wt% (FFB), 0.09 wt% (IND) and 15.1 wt% (IBU) in $TG10_010_010_0$ were predicted. Apparently, the solubility of IND is very low compared to the other APIs. The low solubility of IND in $TG10_010_010_0$ also leads to an almost not existing melting-point depression in the different IND/$TG10_010_010_0$ formulations. Solubility temperatures were found to be

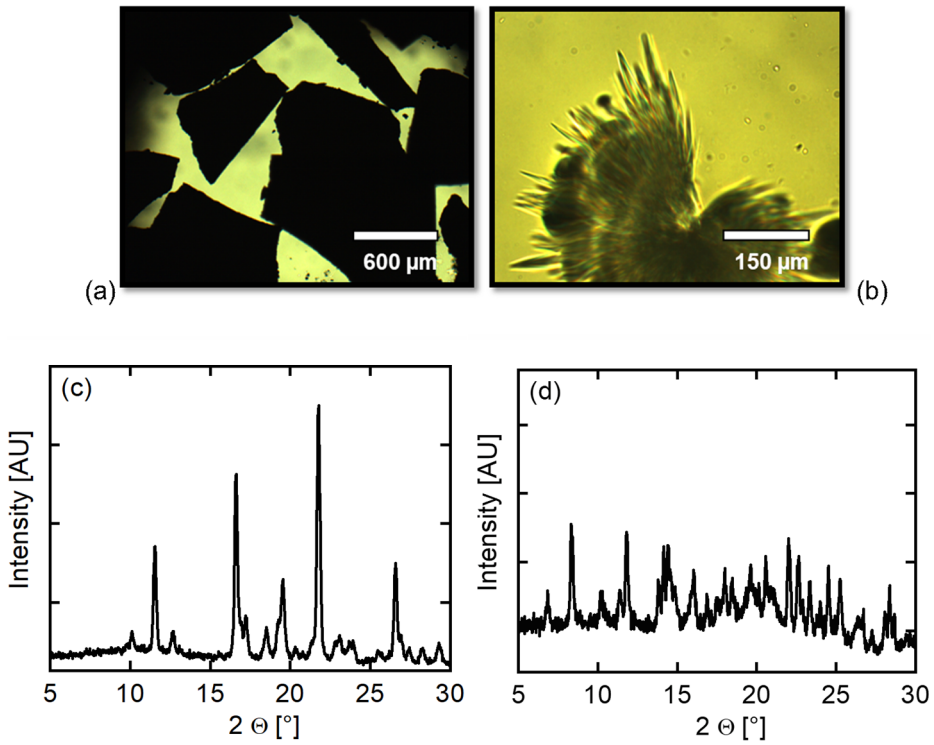

Fig. 3. HSM images (a and b) and PXRD diffractograms (c and d) of the IND/$TG10_010_010_0$ (w_{IND} = 90 wt%) formulation obtained during the first heating ramp at 22 °C (a and c) and obtained after recrystallization during the second heating ramp at 86 °C (b and d).

almost as high as the melting temperature of pure IND.

The solubility of both α- IND and γ-IND in $TG10_010_010_0$ is very well described by PC-SAFT using the same set of parameters (Table 2) only considering the different melting properties of the polymorphs (Table 1). The solubility lines of α-IND and γ-IND never intersect, meaning that γ-IND is the thermodynamically-stable form in the entire temperature/composition range.

The predicted solubility of FFB in $TG10_010_010_0$ (w_{FFB} = 6.8 wt%) at 37 °C agrees with the experimental value (w_{FFB} = 7.4 wt%). Again, DSC and HPLC measurements correspond perfectly.

To illustrate the impact of intermolecular interactions, activity coefficients were calculated for each API in $TG10_010_010_0$ at 25 °C (Fig. 4b). High activity coefficients ($\gamma_{API} > 1$) mean weak molecular interactions between API and TG, whereas small activity coefficients ($\gamma_{API} < 1$) indicate strong molecular interactions between API and TG. Activity coefficients of FFB and IBU in $TG10_010_010_0$ are almost one in the entire composition range (Fig. 4b). This indicates beneficial molecular interactions for FFB/$TG10_010_010_0$ and IBU/$TG10_010_010_0$ and further leads to high API solubilities. Thus, FFB and IBU are API suitable candidates for API/TG formulations from the molecular-interaction point of view. In contrast, IND shows strongly increasing activity coefficients with decreasing IND concentration. The activity coefficients of IND in $TG10_010_010_0$ are even greater than ten at a IND mass fraction of 20 wt% indicating very weak intermolecular interactions between IND and $TG10_010_010_0$. Thus, IND is a less-appropriate candidate for TG-based formulations.

These results emphasize the two main factors determining API solubilities which can be summarized as follows: The melting temperatures and enthalpies of α-IND and γ-IND are high compared to IBU and FFB. Moreover, IND activity coefficients in $TG10_010_010_0$, particularly at low IND concentrations, are very high. Thus, neither the pure-component melting properties nor the intermolecular interactions with TGs are favorable for stable IND/TG formulations. In case of IBU and FFB in $TG10_010_010_0$, activity coefficients are close to one. Considering the favorable activity coefficients and the low melting temperatures and melting enthalpies of IBU and FFB, it can be concluded that TG formulations are favorable for IBU and FFB.

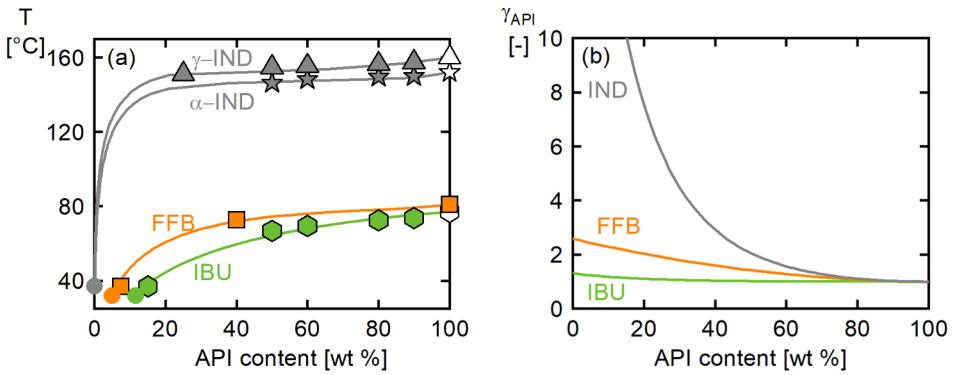

Fig. 4. (a) Solubility of IND, FFB, and IBU in $TG10_010_010_0$. Measured solubilities of IBU (pentagons), FFB (squares), α-IND (stars), γ- IND (triangles). Filled symbols mark experimental results, white symbols are melting points of the pure APIs taken from literature (pentagon [14], star [22], triangle [17]). Circles mark the eutectic temperatures. The solid lines are PC-SAFT calculations. (b) PC-SAFT-calculated activity coefficients of IND, IBU (solid lines), and FFB (dashed line) in $TG10_010_010_0$ at 25 °C.

3.4. Influence of TG C-chain length on API solubility

The fatty-acid chain length is an important characteristic property of TGs. The influence of this chain length on the API solubility was investigated for IBU in $TG8_08_08_0$, $TG10_010_010_0$, and $TG12_012_012_0$. The results are shown in Fig. 5a. Further, Fig. 5b compares the IBU solubility in $TG18_018_018_0$ and $TG16_016_016_0$.

Fig. 5 shows how IBU solubility is influenced by the fatty-acid chain length of the saturated TGs. The solubility was found to slightly increase with increasing fatty-acid chain length of the TGs at elevated temperatures (higher than 40 °C). This in turn leads to lower solubility temperatures, e.g. for a 50 wt% IBU loading in TGs with longer fatty-acid chains: 72.6 °C in $TG8_08_08_0$ vs. 66.8 °C in $TG10_010_010_0$. The chain-length influence becomes negligible for TGs with higher chain lengths. Using the PC-SAFT parameters from Tables 2 and 3, it was possible to predict the solubilities quantitatively correct using the same k_{ij}-value for the various TGs from $TG10_010_010_0$ to $TG18_018_018_0$. The results of the different experimental procedures agree very well. At 25 °C, the solubility of IBU in $TG8_08_08_0$ was found to be 9.6 wt% according to the HPLC measurement and 9.4 wt% according to the Raman measurement. It revealed that the literature values from Hong et al. [12] slightly deviate from the modeling and the experimental data obtained in this work. The small differences may originate from several reasons: melting temperatures were not extrapolated to a theoretical ramp of 0 K min^{-1} in the work of Hong et al. This may result in a small shift of the melting temperatures due to kinetic effects in the DSC pan. Further, IBU was obtained from a different supplier in this work, which also might affect the melting properties of the investigated IBU.

The eutectic points strongly increase with increasing chain length of the TGs. Only for IBU/$TG8_08_08_0$, the eutectic point lies below room temperature (8.1 wt% at T_{eut} = 11.5 °C). Thus a stable liquid IBU/TG mixture can only be realized using $TG8_08_08_0$ and only containing a maximum IBU content of about 9.6 wt%. IBU in $TG10_010_010_0$ will crystallize at room temperature (T_{eut} = 31.9 °C) at any composition. An IBU/$TG10_010_010_0$ mixture becomes liquid at 37 °C body temperature unless the IBU/TG mixture exceeds a maximum IBU-content of 13.2 wt %. IBU in $TG12_012_012_0$ will always be fully crystalline (T_{eut} = 42.38 °C) at body temperature. Therefore the latter combination is inappropriate for any liquid formulation at body or room temperature although it shows higher IBU solubilities than $TG8_08_08_0$ and $TG10_010_010_0$ above the eutectic points. The eutectic compositions are shifted more to the IBU-rich side for both IBU/$TG18_018_018_0$ ($w_{IBU,eut}$ = 40.7 wt%) and IBU/$TG16_016_016_0$ ($w_{IBU,eut}$ = 32.9 wt%) and are located at even higher temperatures ($TG18_018_018_0$: T_{eut} = 65.5 °C, $TG16_016_016_0$: T_{eut} 59.7 °C) (see Fig. 5b). For that reason, the solubility was measured only for IBU/$TG8_08_08_0$ at 25 °C. For all other TGs shown in Fig. 5, the eutectic temperature is higher and therefore solubility measurements cannot be performed at 25 °C.

Thus, the TG chain length has a strong impact on the eutectic temperature of binary API/TG mixtures. Saturated TGs with fatty-acid chain lengths greater than 10 carbon atoms are apparently not reasonable for formulating the APIs considered in this work.

3.5. Influence of TG degree of saturation on API solubility

The influence of the TGs degree of saturation on the API solubility was investigated by comparing TGs with the same fatty-acid chain lengths (18 carbon atoms) and different degree of saturation, namely one completely-saturated TG ($TG18_018_018_0$) and two unsaturated TGs ($TG18_118_118_1$ and $TG18_218_218_2$). For APIs in unsaturated TGs, only the solubility line of the API was calculated as no eutectic temperatures were measured for these systems. Fig. 6 shows the solubilities of IBU (Fig. 6a) and FFB (Fig. 6b) in these TGs.

The occurrence of unsaturated C-chains in TG fatty acids dramatically influences the eutectic points (Fig. 6). The melting points of those components lie distinctively below room temperature and therefore enable formulation of stable, liquid API/TG mixtures at 25 °C. The experimental DSC results and the PC-SAFT modeled solubility lines are almost identical for IBU in both unsaturated TGs ($TG18_118_118_1$ and $TG18_218_218_2$).

At 25 °C, the solubility of IBU in $TG18_118_118_1$ and $TG18_218_218_2$, is calculated to be w_{IBU} = 4.0 wt% and is thus equals the solubility of FFB in $TG18_118_118_1$ (4.2 wt%) and $TG18_218_218_2$ (3.9 wt%). The solubilities of the APIs only slightly differ for $TG18_118_118_1$ and $TG18_218_218_2$, and are in very good agreement with the PC-SAFT calculations (e.g. 2.8 wt% for FFB in $TG18_118_118_1$ and 3.9 wt% for FFB in $TG18_218_218_2$).

Above the eutectic temperature of IBU/$TG18_018_018_0$ at 65.5 °C, the solubility of IBU is significantly higher in $TG18_018_018_0$ compared to $TG18_118_118_1$ and $TG18_218_218_2$. This implies that IBU has higher solubilities in saturated TGs compared to the unsaturated ones. Further, there is no distinctive difference between the solubility lines of IBU in $TG18_118_118_1$ and $TG18_218_218_2$ which implies that the degree of saturation has only a minor effect on the IBU solubility.

This significantly-higher solubility in saturated TGs was not observed in case of FFB/TG mixtures (Fig. 6b). In the case of FFB, all three solubility lines lie almost above each other (Fig. 6b) and do not deviate as strong as for IBU (Fig. 6a). The influence of TG degree of saturation is obviously different for different APIs. This arises from differently-strong interactions (e.g. association and van der Waals interactions) with the different functional groups of the APIs and does not allow for general conclusions regarding the solubility of APIs in TGs. However, differently-strong interactions are explicitly considered by the physically-sound thermodynamic model PC-SAFT which allows modeling the different solubility behaviors. Fig. 7 displays the activity coefficients of IBU in $TG18_018_018_0$, $TG18_118_118_1$ and $TG18_218_218_2$ at 25 °C.

In each TG, the IBU activity coefficients increase with decreasing IBU content. Activity coefficients are lowest in IBU/$TG18_018_018_0$ which corresponds to the increased solubility of IBU in saturated

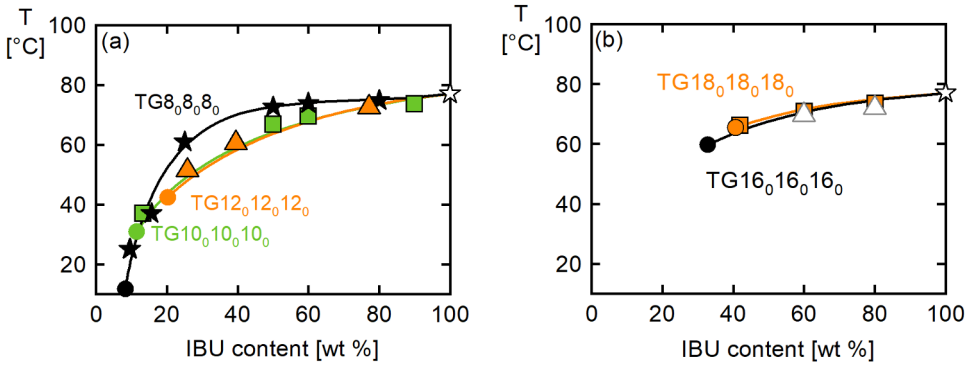

Fig. 5. (a) Solubility of IBU in $TG8_08_08_0$ (stars), $TG10_010_010_0$ (squares, see Fig. 4a), and $TG12_012_012_0$ (triangles). Circles are PC-SAFT calculated eutectic points, the white star is the pure melting temperature of pure IBU from literature [14]. Lines stand for PC-SAFT calculations. The predicted solubility lines of IBU in $TG10_010_010_0$ and $TG12_012_012_0$ are almost identical and therefore hard to distinguish. (b) Solubility of IBU in $TG18_018_018_0$ and $TG16_016_016_0$. Squares are experimental values, the white star marks the melting point of pure IBU [14], white triangles are literature solubility values for IBU in $TG16_016_016_0$ [12]. Circles are the eutectic points in $TG16_016_016_0$ and $TG18_018_018_0$, respectively. Lines are PC-SAFT calculations.

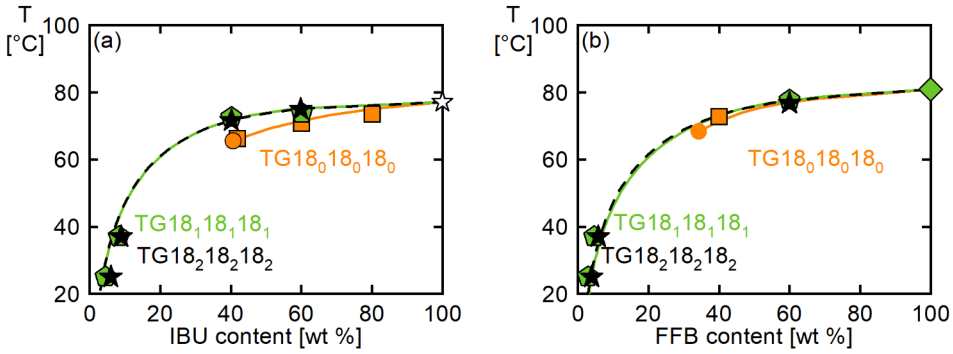

Fig. 6. Solubility of (a) IBU and (b) FFB in $TG18_0 18_0 18_0$, $TG18_1 18_1 18_1$ and $TG18_2 18_2 18_2$. Symbols represent measurements in various TGs (squares: $TG18_0 18_0 18_0$, pentagons: $TG18_1 18_1 18_1$, stars: $TG18_2 18_2 18_2$,). White star is the pure melting point of IBU from literature [14]. The diamond marks the melting point of pure FFB. Circles are the eutectic points of the API/$TG18_0 18_0 18_0$ mixture. Lines are PC-SAFT calculations.

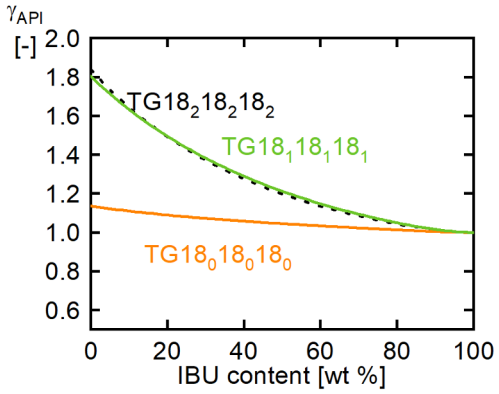

Fig. 7. Activity coefficients of IBU in $TG18_0 18_0 18_0$, $TG18_1 18_1 18_1$ (solid lines) and $TG18_2 18_2 18_2$ (dashed line) calculated with PC-SAFT at 25 °C.

$TG18_0 18_0 18_0$ compared to the ones in $TG18_1 18_1 18_1$ and $TG18_2 18_2 18_2$. Activity coefficients of IBU in $TG18_1 18_1 18_1$ and $TG18_2 18_2 18_2$ lie on one line, reflecting the IBU similar solubility results from Fig. 6a and the favorable intermolecular interactions between IBU and TGs.

For the investigated API/TG mixtures a formulation that is liquid at room temperature can only be created by using either a TG with medium C-chain ($TG8_0 8_0 8_0$) or a TG with unsaturated fatty-acids ($TG18_1 18_1 18_1$ or $TG18_2 18_2 18_2$). The solubility of IBU (10.5 wt%) and FFB (9.5 wt%) in the saturated, medium-chained $TG8_0 8_0 8_0$, was found to be higher compared to the solubilities in the unsaturated TGs (≈4.0 wt%). Therefore, we recommend to use $TG8_0 8_0 8_0$ for lipid formulations of the investigated APIs, if solubility has to be maximized. This is in agreement with findings from recent works, in which mixed saturated medium-chained TGs and mixed unsaturated long-chained TGs have been compared [9,31].

3.6. API solubility in TG mixtures

The adequate description of API solubility in TG mixtures using PC-SAFT was investigated for IBU in a binary mixture of 20 wt% $TG10_0 10_0 10_0$ and 80 wt% $TG8_0 8_0 8_0$. Fig. 8a shows the solubility of $TG10_0 10_0 10_0$ in $TG8_0 8_0 8_0$. Fig. 8b shows the solubility of IBU in the before-mentioned TG mixture.

It can be seen in Fig. 8a that a mixture of 20 wt% $TG10_0 10_0 10_0$ and 80 wt% $TG8_0 8_0 8_0$ is liquid at 25 °C (the solubility temperature of a this mixture is 17.3 °C according to the measurement and 18.9 °C according to the PC-SAFT prediction). Based on this finding, a mixture with 20 wt % $TG10_0 10_0 10_0$ was chosen for preparing a liquid IBU/TG mixture. Two mixtures with 50 wt% IBU and 60 wt% IBU were ball milled and their solubility temperatures were determined with DSC (Fig. 8b). The predicted solubility line of this IBU/TG mixture lies between the solubility lines of IBU in the two pure TGs and perfectly corresponds with the DSC data (measurement results summarized in Table S1 of the supplement). The calculated IBU solubility at 25 °C is 10.5wt%, which is almost the same value as obtained for IBU in $TG8_0 8_0 8_0$ (w_{IBU} = 10.1 wt%). Mixtures of $TG8_0 8_0 8_0$ and $TG10_0 10_0 10_0$ do thus obviously not enhance the IBU solubility at room temperature.

4. Conclusions

In this work, DSC, HSM, HPLC, and Raman spectroscopy experiments were combined with thermodynamic modeling to determine solubilities of APIs in pure TGs and a binary mixture of $TG8_0 8_0 8_0$ and $TG10_0 10_0 10_0$. Activity coefficients of APIs in TGs taking into account the intermolecular interactions between APIs and TGs were calculated at 25 °C. They were found to strongly depend on the type of API and impact their solubility (besides the melting properties of the pure API). While IND revealed to be inappropriate for binary API/TG formulations with $TG10_0 10_0 10_0$ due to both, its melting properties and the weak interactions with TGs, FFB and IBU seem to be better suitable for LBDDS formulations.

The length of the C-chains in the TGs was found to have only a

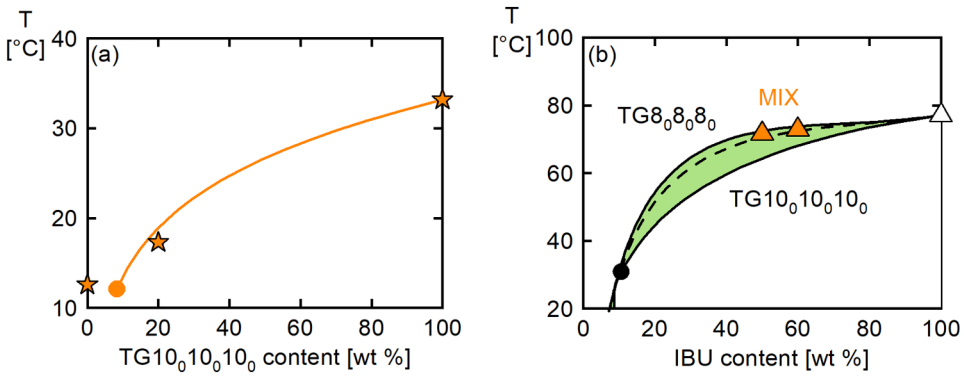

Fig. 8. (a) Solubility of $TG10_0 10_0 10_0$ in $TG8_0 8_0 8_0$. Stars are experimental values and the circle marks the eutectic point. The solid line is the solubility line predicted with PC-SAFT. (b) Solubility of IBU in a $TG8_0 8_0 8_0$/$TG10_0 10_0 10_0$ mixture. Filled triangles are experimental values and the white triangle is a literature value for pure IBU [14]. The circle marks the eutectic point of IBU/$TG10_0 10_0 10_0$. The dashed line is the PC-SAFT prediction for IBU solubility in a mixture containing 80 wt% $TG8_0 8_0 8_0$ and 20 wt% $TG10_0 10_0 10_0$. The solid lines are modeling results for IBU in $TG8_0 8_0 8_0$ and $TG10_0 10_0 10_0$ from Fig. 5. The filled area indicates the solubility area of IBU in different $TG8_0 8_0 8_0$/$TG10_0 10_0 10_0$ mixtures.

minor impact on the solubility of the APIs considered in this work. The eutectic temperatures of the API/TG mixtures increased remarkably with increasing TG chain length. In case of IBU and FFB, only the unsaturated, long-chained TGs $TG18_118_118_1$ and $TG18_218_218_2$ as well as the saturated, medium-chained $TG8_08_08_0$ possess eutectic points below 25 °C. Thus, saturated TGs with chain lengths greater than ten carbon atoms are unfavorable TGs for formulating stable liquid formulations at room temperature. Main factor influencing the API solubility in a pure TG was found to be TG saturation. At 25 °C, the solubility of IBU and FFB was approximately half as high in the unsaturated $TG18_118_118_1$ and $TG18_218_218_2$ compared to the one in the saturated $TG8_08_08_0$.

It could be seen that API/TG interactions in API/TG mixtures strongly depend on the chosen API. The determination of activity coefficients was proven being a useful tool for predicting those intermolecular interactions. Beneficial intermolecular interactions were found for TGs with IBU and FFB, whereas weak interactions were found for TGs with IND. Thermodynamic modeling via PC-SAFT thus enables screening for suitable API/TG combinations and moreover also for predicting the API solubilities in TG mixtures.

Acknowledgements

This work has been supported by Deutsche Forschungsgemeinschaft (DFG) with Grant SA700/20 (Gottfried Wilhelm Leibniz Prize awarded to Gabriele Sadowski).

Appendix A. Supplementary material

Supplementary data to this article can be found online at https://doi.org/10.1016/j.ejpb.2019.10.012.

References

[1] S. Kalepu, V. Nekkanti, Insoluble drug delivery strategies: review of recent advances and business prospects, Acta Pharm. Sin. B 5 (2015) 442–453.
[2] M. Kuentz, Lipid-based formulations for oral delivery of lipophilic drugs, Drug Discov. Today. Technol. 9 (2012) e97–e104.
[3] C.W. Pouton, Lipid formulations for oral administration of drugs: non-emulsifying, self-emulsifying and 'self-microemulsifying' drug delivery systems, Eur. J. Pharm. Sci. 11 (Suppl 2) (2000) S93–S98.
[4] F.D. Gunstone, Vegetable Oils in Food Technology: Composition, Properties and Uses, second ed., Wiley-Blackwell, Chichester, 2011.
[5] L.C. Alskär, C.J.H. Porter, C.A.S. Bergström, Tools for early prediction of drug loading in lipid-based formulations, Mol. Pharm. 13 (2016) 251–261.
[6] C.W. Pouton, Formulation of poorly water-soluble drugs for oral administration: physicochemical and physiological issues and the lipid formulation classification system, Eur. J. Pharm. Sci. 29 (2006) 278–287.
[7] F. Ditzinger, D.J. Price, A.-R. Ilie, N.J. Köhl, S. Jankovic, G. Tsakiridou, S. Aleandri, L. Kalantzi, R. Holm, A. Nair, C. Saal, B. Griffin, M. Kuentz, Lipophilicity and hydrophobicity considerations in bio-enabling oral formulations approaches - a PEARRL review, J. Pharm. Pharmacol. 71 (2018) 1–19.
[8] T.D. Thi, M. van Speybroeck, V. Barillaro, J. Martens, P. Annaert, P. Augustijns, J. van Humbeeck, J. Vermant, G. van den Mooter, Formulate-ability of ten compounds with different physicochemical profiles in SMEDDS, Eur. J. Pharm. Sci. 38 (2009) 479–488.
[9] L.C. Persson, C.J.H. Porter, W.N. Charman, C.A.S. Bergström, Computational prediction of drug solubility in lipid based formulation excipients, Pharm. Res. 30 (2013) 3225–3237.
[10] N. Gautschi, C.A.S. Bergström, M. Kuentz, Rapid determination of drug solubilization versus supersaturation in natural and digested lipids, Int. J. Pharm. 513 (2016) 164–174.
[11] T.J. Dening, S. Rao, N. Thomas, C.A. Prestidge, Montmorillonite-lipid hybrid carriers for ionizable and neutral poorly water-soluble drugs: formulation, characterization and in vitro lipolysis studies, Int. J. Pharm. 526 (2017) 95–105.
[12] J. Hong, D. Hua, X. Wang, H. Wang, J. Li, Solid − liquid − gas equilibrium of the ternaries ibuprofen + myristic acid + CO 2 and ibuprofen + tripalmitin + CO 2, J. Chem. Eng. Data 55 (2010) 297–302.
[13] B.D. Anderson, M.T. Marra, Chemical and related factors controlling lipid solubility, Bull. Tech. Gattefosse 92 (1999) 11–19.
[14] C. Luebbert, F. Huxoll, G. Sadowski, Amorphous-amorphous phase separation in API/polymer formulations, Molecules 22 (2017) 296.
[15] K. Lehmkemper, S.O. Kyerematen, M. Degenhardt, G. Sadowski, Influence of low-molecular-weight excipients on the phase behavior of PVPVA64 amorphous solid dispersions, Pharm. Res. 35 (2018) 25.
[16] J. Brinkmann, C. Luebbert, D.H. Zaitsau, S.P. Verevkin, G. Sadowski, Thermodynamic modeling of triglycerides using PC-SAFT, J. Chem. Eng. Data 64 (2019) 1446–1453.
[17] A. Prudic, Y. Ji, G. Sadowski, Thermodynamic phase behavior of API/polymer solid dispersions, Mol. Pharm. 11 (2014) 2294–2304.
[18] C. Luebbert, C. Klanke, G. Sadowski, Investigating phase separation in amorphous solid dispersions via Raman mapping, Int. J. Pharm. 535 (2018) 245–252.
[19] J.M. Prausnitz, Molecular Thermodynamics of Fluid-Phase Equilibria, third ed., Prentice Hall, New Jersey, 1999.
[20] J. Gross, G. Sadowski, Perturbed-chain SAFT: an equation of state based on a perturbation theory for chain molecules, Ind. Eng. Chem. Res. 40 (2001) 1244–1260.
[21] G.H. Charbonnet, W.S. Singleton, Thermal properties of fats and oils, J. Am. Oil Chem. Soc. 24 (1947) 140–142.
[22] X. Pan, T. Julian, L. Augsburger, Increasing the dissolution rate of a low-solubility drug through a crystalline-amorphous transition: a case study with indomethacin correction of indomethicin, Drug Dev. Ind. Pharm. 34 (2008) 221–231.
[23] J. Gross, G. Sadowski, Application of the perturbed-chain SAFT equation of state to associating systems, Ind. Eng. Chem. Res. 41 (2002) 5510–5515.
[24] M. Kleiner, G. Sadowski, Modeling of polar systems using PCP-SAFT: an approach to account for induced-association interactions, J. Phys. Chem. C. 111 (2007) 15544–15553.
[25] E. Altuntepe, A. Reinhardt, J. Brinkmann, T. Briesemann, G. Sadowski, C. Held, Phase behavior of binary mixtures containing succinic acid or its esters, J. Chem. Eng. Data 62 (2017) 1983–1993.
[26] S. Watterson, S. Hudson, M. Svärd, Å.C. Rasmuson, Thermodynamics of fenofibrate and solubility in pure organic solvents, Fluid Phase Equilib. 367 (2014) 143–150.
[27] F. Ruether, G. Sadowski, Modeling the solubility of pharmaceuticals in pure solvents and solvent mixtures for drug process design, J. Pharm. Sci. 98 (2009) 4205–4215.
[28] D. Novakovic, A. Isomäki, B. Pleunis, S.J. Fraser-Miller, L. Peltonen, T. Laaksonen, C.J. Strachan, Understanding dissolution and crystallization with imaging: a surface point of view, Mol. Pharm. 15 (2018) 5361–5373.
[29] S.A. Surwase, J.P. Boetker, D. Saville, B.J. Boyd, K.C. Gordon, L. Peltonen, C.J. Strachan, Indomethacin: new polymorphs of an old drug, Mol. Pharm. 10 (2013) 4472–4480.
[30] L. Lange, G. Sadowski, Polymorphs, hydrates, cocrystals, and cocrystal hydrates: thermodynamic modeling of theophylline systems, Cryst. Growth Des. 16 (2016) 4439–4449.
[31] H.D. Williams, P. Sassene, K. Kleberg, J.-C. Bakala-N'Goma, M. Calderone, V. Jannin, A. Igonin, A. Partheil, D. Marchaud, E. Jule, J. Vertommen, M. Maio, R. Blundell, H. Benameur, F. Carrière, A. Müllertz, C.J.H. Porter, C.W. Pouton, Toward the establishment of standardized in vitro tests for lipid-based formulations, part 1: method parameterization and comparison of in vitro digestion profiles across a range of representative formulations, J. Pharm. Sci. 101 (2012) 3360–3380.